# Non-contact acoustic method for the simultaneous measurement of thickness and acoustic properties of biological tissues

**H. Okawai*†, M. Tanaka* and F. Dunn‡**

* Research Institute for Chest Diseases and Cancer, Tohoku University, 4-1 Seiryo-machi, Sendai 980, Japan
† Medical Engineering Laboratory, Sendai Kosei Hospital, 4 Hirosemachi, Sendai 980, Japan
‡ Bioacoustics Research Laboratory, University of Illinois, 1406 West Green Street, Urbana, Illinois 61801, USA

*Received 18 September 1989*

The frequency dependence of the magnitude and phase shift of reflected waves from a thin tissue specimen has been found to yield characteristic patterns as a function of the specimen thickness. By analysis of those characteristic patterns, the specimen thickness can be determined so that the attenuation constant and the sound speed can be obtained by a non-contact procedure. The method is demonstrated in the frequency range 100 MHz to 200 MHz, using a scanning acoustic microscope and approximately 10 $\mu$m thick myocardial tissue samples of human origin, one paraffin embedded.

**Keywords: biological tissues; measurement; acoustic properties**

## Introduction

Generally, two approaches can be considered for the investigation of structural features of tissues, as shown in *Figure 1*. In the method illustrated by *Figure 1a*, the average and/or summation of properties of various tissue elements is observed because the dimensions of the acoustic beam width are larger than those of the individual tissue elements. On the other hand, such structure elements can be observed microscopically, as suggested in *Figure 1b*.

The acoustic microscope has been applied to make observations at the microscopic level and some of the acoustic properties of tissues have been obtained with the scanning laser acoustic microscope (SLAM)[1,2]. Usually, the thickness of a specimen is determined by placing it between two solid plates with parallel contact surfaces of known spearation. In the SLAM, a specimen is placed between a substrate and a cover slip with the spacing distance determined by a spacer of known dimension so that precise values of specimen thickness are obtained.

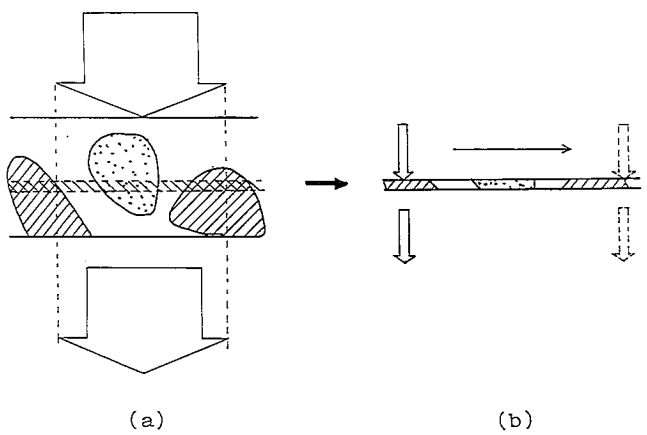


**Figure 1** Two methods for measuring acoustic propagation properties of biological tissues: (a) average or sum of numerous tissue elements and (b) individual tissue elements

In pathology and histology, tissue specimens less than 10 $\mu$m in thickness are generally examined with the light microscope. It is thin tissue sections such as these that we wish to investigate acoustically. However, the contact methods described above cannot be employed readily for such thin tissues with sufficient accuracy, because the surface of such a thin tissue slice cannot be assumed to be microscopically flat and because details of contact of the tissue specimen to solid plates are unknown.

Lee *et al.*[3] studied a non-contact measuring method for thin metal films by analysing the interference of sound waves produced on interfaces spaced the thickness of the film, and it would be desirable to have available such a non-contact method applicable to thin biological tissue sections. In the present study a non-contact method, which utilizes this interference of sound waves, was developed for determining the thickness, attenuation constant and sound speed of thin biological tissue specimens. Though this method was reported earlier[4,5] it is described completely here.

The frequency characteristics of the reflection coefficient of a thin tissue specimen mounted on a glass substrate, to comprise a three layered structure (coupling medium/tissue/substrate), is first discussed for focused waves in the frequency range 100 MHz to 200 MHz of the scanning acoustic microscope (SAM). It is shown that the reflection coefficient gives characteristic patterns as a function of

specimen thickness, and that the specimen thickness can be determined from these characteristic patterns to yield the attenuation constant and sound speed of a tissue element by a non-contact procedure.

## Measurement method

### *Instrumentation*

The SAM system employed in this study is based on the instrumentation of Lemons and Quate[6], and has been developed for applications in medicine and biology[7,8], as shown schematically in *Figure 2*. The transducer has been described by Chubachi *et al.*[9]. The acoustic focusing element comprises a ZnO piezoelectric transducer with a sapphire lens, for which the aperture half angle is 30° and which focuses the acoustic beam with the lateral resolution, 1/2 power width, from approximately 6 $\mu$m at 200 MHz to 12 $\mu$m at 100 MHz, in water at 20°C. *Figure 3* shows the relative reflected power profile along the beam axis ($Z$) in the neighbourhood of the focal zone, as determined from the measurements of the amplitude of the received signal reflected from a plane glass surface. Thus, the magnitude of the reflected wave depends upon position along the beam axis. The focusing element is mechanically scanned at 60 Hz, in the lateral direction ($X$) above the specimen, which remains stationary on the specimen holder, while the holder is scanned in the other lateral direction ($Y$) in 8 s, thus providing two-dimensional scanning. Images of amplitude, phase and interference are obtained in a field of view 2 mm × 2 mm. The amplitude and phase images are displayed in colour scales of at most of 16 shades. *Figure 4* is an example of a display of 16 shades of grey. The detailed quantitative values of the tissue elements in these two images are obtained from line scans of each profile along the $X$ direction, as shown by the white lines in the figure.

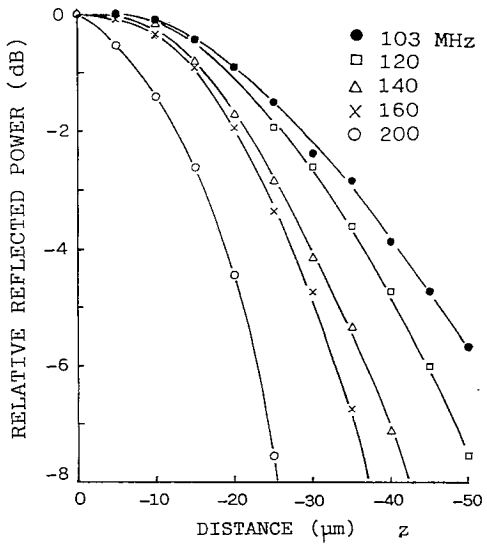


**Figure 3** Relative reflected power profile along the beam axis determined from the amplitude of the received wave reflected from a glass substrate. The focal point is at $z = 0$

## Components of reflected waves

The focused wave was used in the reflection mode and components of reflected waves were studied to establish a method for the determining acoustic properties with usable accuracy. The wave was positioned with the focal point on the glass substrate surface, as shown in *Figure 5a*. The incident angles of the waves vary between 0° and 30°. As the maximum angle is 30°, surface waves (mode conversion) do not occur, in principle, at the interfaces between the coupling medium and tissue (sound speed: approximately 1500 m/s) or between the glass substrate (2400 m/s) and tissue (see *Table 1*).

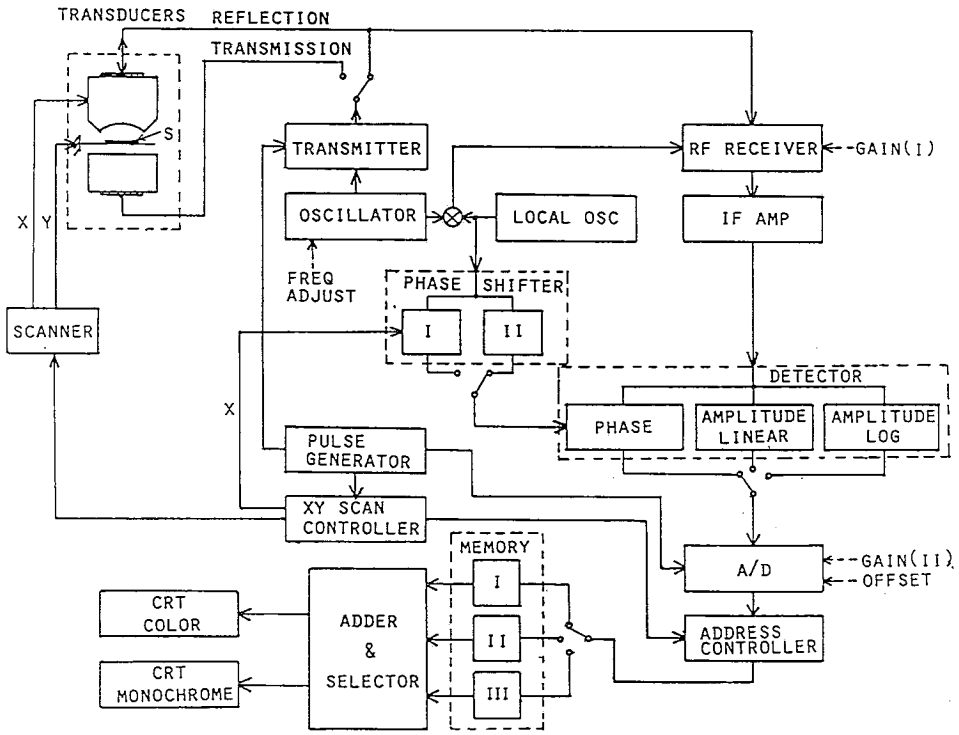


**Figure 2** Block diagram of the mechanically scanned acoustic microscope (SAM) (after reference 8, revised)

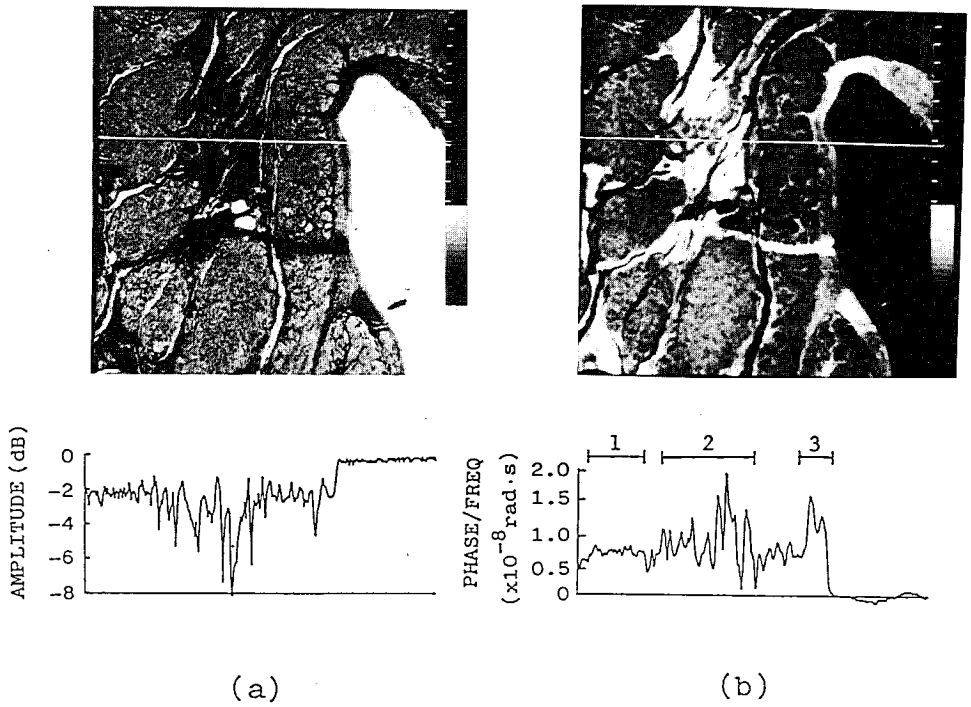


**Figure 4** SAM images (a) amplitude; (b) phase, and A-mode profiles for the sample represented in *Figure 11* (at 20°C). The samples are around 10 $\mu$m thick and are sectioned from three infarcted myocardia. A-mode graphs show amplitude and phase profiles along the white lines. On the plot in (b) the area under bar 1: normal cardiac muscles area; area under bar 2: collagenous changed area; area under bar 3: elastic changed area

Consider first the wave at $\theta_j = 0$. In *Figure 5a*, the reflection coefficients in the following two cases agree to less than 1% difference, that is, the reflected pressure wave is considered as the sum of the wave reflected from the surface of the tissue specimen $y_s$, the round trip wave in the tissue $y_a$, and the twice round trip wave $y_b$, as compared with the sum of the many reflected waves embodied in the reflection coefficient for normal incidence. Secondly, consider the three instantaneous pressure components $y_s$, $y_a$ and $y_b$ for incidence at angle $\theta_j$, and consider further that the radius of curvature $R$ of the lens is much greater than the specimen thickness $l_0$, i.e., $R \gg l_0$. Thus, the portion of the lens at which the waves $y_s$, $y_a$ and $y_b$ are incident can be considered plane (See *Figure 5c*). Therefore, the reflected wave $y_r$ can be taken as

$$y_r = y_s + y_a + y_b \tag{1}$$

for the condition that the incident wave $|y_i| = 1$, that is, the wave quantities $y_s$, $y_a$ and $y_b$ are reflection coefficients, as illustrated in *Figure 5a*, and are given by

$$y_s = R_{12} \exp(-2\gamma_1(R-l)) \tag{2}$$

$$y_a = T_{12}R_{23}T_{21} \exp(-2\gamma_1(R-l)) \exp(-2\gamma_2 l) \tag{3}$$

$$y_b = T_{12}R_{23}R_{21}R_{23}T_{21} \exp(-2\gamma_1(R-l)) \exp(-4\gamma_2 l) \tag{4}$$

where $R_{ij}$ and $T_{ij}$ are the coefficients of reflection and transmission, respectively, for which $i$ and $j$ correspond, respectively, to the incident and transmitted components. The path length $l_1$, and the propagation constants $\gamma_1$ and $\gamma_2$ are given by

$$l = l_0/\cos\theta_j, \tag{5}$$

$$\gamma_1 = j\beta_1 \tag{6}$$

$$\gamma_2 = \alpha_2 + j\beta_2. \tag{7}$$

The area $ds$ at the distance of $l_0$ from the focal point, as shown in *Figure 5b*, is

$$ds = 2\pi l \sin\theta_j \, dh \tag{8}$$

where the incident angle $\theta_j$ and the width of the wave element ring $dh$ are determined by $N$, the total number of angular fractions that the aperture half angle ($\pi/6$) is subdivided, for computer calculation, as given by

$$\theta_j = \pi j/6N \tag{9}$$

$$dh \simeq l(\pi/6N) \tag{10}$$

From equations (8)–(10), $ds$ is

$$ds = \pi^2 l^2 \sin\theta_j/3N \tag{11}$$

Consequently, the received wave $y$ is given by

$$y = \sum_{j=0}^{N-1} y_r ds$$

$$= \sum_{j=0}^{N-1} y_r(\pi^2 l^2 \sin\theta_j/3N) \tag{12}$$

The acoustic intensity attenuation $L$ for the reduction in the reflected wave is given by

$$L = -(10 \log y^2 - 10 \log R_{23}^2) \tag{13}$$

where the second term on the right hand side accounts for the reflection loss at the boundary between media II and III.

The phase shift for the case without a tissue specimen present is

$$y_{r\,ref} = R_{13} \exp(-2\beta_1 R) \tag{14}$$

so that the reference wave $y_{ref}$ is, from equation (12),

$$y_{ref} = \sum_{j=0}^{N-1} y_{r\,ref}(\pi^2 l^2 \sin\theta_j/3N) \tag{15}$$

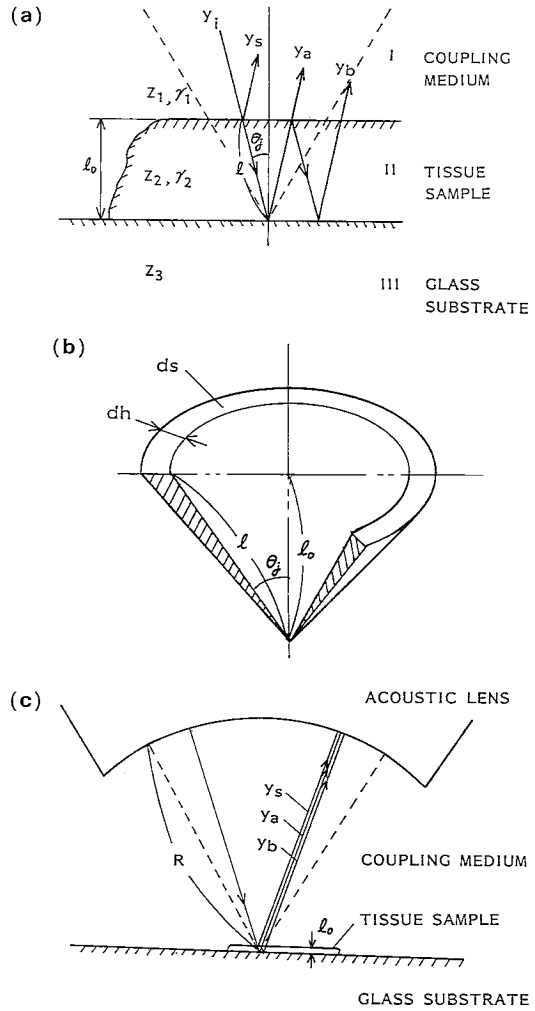


**Figure 5** Acoustic model for a focused wave and a specimen. (a) Acoustic components of reflected waves from a tissue mounted on a glass substrate. $Z_1, Z_2, Z_3$: acoustic impedances; $\gamma_1, \gamma_2$: propagation constants. The suffixes 1, 2 or 3 correspond to medium I, II or III, respectively. $l_0$: specimen thickness ($\simeq 10$ $\mu$m). $\theta_j$: aperture half angle, 0° to 30°. Radius of curvature $R$ of the lens is approximately 1.5 mm. (b) An acoustic model to discuss an 'annular wave element'. (c) Paths of the receiving waves $y_a$, $y_b$, $y_c$. $R = 1.5$ mm, $l_0 \simeq 10$ $\mu$m. Dashed lines show beamwidth

and the phase shift $\phi$ is

$$\phi = \arg(y/y_{ref}) \tag{16}$$

*Figure 6a* shows the calculation of attenuation and phase shift using 1600 m/s and 100 dB mm$^{-1}$ (at 100 MHz), respectively, for the sound speed $C_s$ and the attenuation constant of medium II, in equations (12)–(16), under the assumption that the frequency exponent $n$ is unity, in the attenuation coefficient $\alpha = Af^n$ (neper m$^{-1}$), and that the sound speed is non-dispersive. The constant $A = 100 \times 1000/(8.686 \times 100 \times 10^6) = 1.15 \times 10^{-4}$ (neper s m$^{-1}$), using the constants above. The speed scale on the right side of the phase graph, is determined by

$$C_s = \frac{1}{\frac{1}{C_w} - \frac{\phi}{f} \times \frac{1}{4\pi l_0}} \tag{17}$$

where $C_w$ is sound speed of the coupling medium (water at 20°C), and $f$ is ultrasound frequency in hertz, $\phi$ is the phase shift of the round trip wave for $y_a$ at $\theta_j = 0$. In *Figure 6*, compared with the traces for $y_r = y_s + y_a + y_b$, the traces for $y_r = y_s + y_a$ have greater undulation amplitude in attenuation and less undulation amplitude in phase shift. It is also seen that the sound speed for the round trip wave $y_a$, calculated between the angles 0° to 30°, is greater than 1600 m s$^{-1}$ by approximately 6 m s$^{-1}$, but that the variation in attenuation between the value for the round trip wave $y_a$ at angles 0° to 30°, and the value for $\theta_j = 0$ is not apparent from the figure as they are less than $10^{-3}$ dB.

For the case where the wave is the summation in the range of $j$ between 0 to 40 ($N = 64$), that is, the aperture half angle is approximately 19°, the attenuation and phase shift are shown in *Figure 6b*, where the sound speed of $y_a$ is taken as 1600 m s$^{-1}$, and undulation pattern agrees for $\theta_j = 0$.

*Figure 7a* and *b* shows examples of measurement for a stomach cancer (curve A) and a normal rat liver (curve B). *Figure 7c* and *d* illustrates the calculation using the specific values given in the figure title. The values for curves A and B are in the range $j = 0$ to 40 (0° to approximately 19°) and 0 to 32 (0° to 15°), respectively. As a result, the magnitude of the undulation in attenuation appears in the same way as $y_s + y_a$ but the traces for phase shift do not allow the $y_s + y_a + y_b$ wave and the $y_s + y_a$ wave to be distinguished as they exhibit nearly identical patterns. It may be possible to consider that the received wave is a summation of $y_s$ and $y_a$. The measurement data (*Figure 7a* and *b*) agree well with the calculation (*Figure 7c* and *d*) under the assumption that the aperture half angle is less than 30°. Also it is considered that the angle becomes small with increasing sound speed because incident waves of large angles are refracted out of the region of the reception. As shown in *Figure 3*, the focal zone varies with frequency, suggesting that there are more wave components of large incident angle in the high frequency region than in the low frequency region.

*Figure 8* shows reflection coefficients of a polyester film (Diafoil Company, Tokyo, Japan), mounted on a glass

**Table 1** Acoustic constants and notations (after reference 5)

| | Coupling medium (water 20°C) | Sample (tissue) | Sample mounting (slide glass) |
|---|---|---|---|
| Sound speed (m s$^{-1}$) | $C_w = 1483$* | $C_s$ | |
| Density (g cm$^{-3}$) | 0.9983 | $\rho = 1.06$ | |
| Acoustic impedance (kg m$^{-2}$ s$^{-1}$) | $Z_1 = 1.480 \times 10^6$ | $Z_2 = \rho C_s$ | $Z_3 = 17 \times 10^6$ |
| Phase constant (radian m$^{-1}$) | $\beta_1$ | $\beta_2$ | |
| Attenuation constant (neper m$^{-1}$) | | $\alpha_2$ | |

* Data from ref. 16

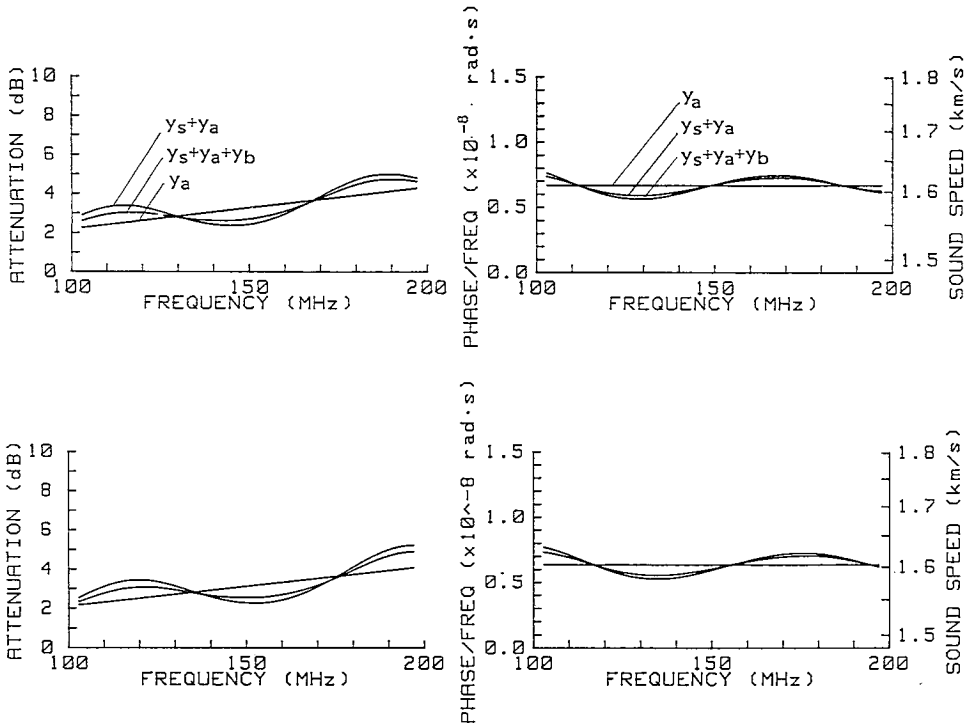


**Figure 6** Calculation of attenuation and phase shift. (a) Angle $\theta_j$ range 0° to 30°. $C_s$: sound speed, 1600 m s$^{-1}$. (b) Angle $\theta_j$ range 0° to 19°

substrate. The film thickness of 37.0 $\mu$m was measured with a tool for thickness measurement (Mu-Checkers M300, Mitutoyo Mfg, Tokyo, Japan). Sound speed and acoustic impedance were measured to be 2400 m s$^{-1}$ at 24°C and $3.35 \times 10^6$ kg m$^{-2}$ s$^{-1}$, respectively. The constants $A$ and $n$ in the equation of the frequency dependence of the attenuation coefficient, $\alpha = Af^n$ (neper m$^{-1}$), were determined to be $A = 2 \times 10^{-14}$ to $5 \times 10^{-14}$ and $n = 2$. The sound speed value agrees well with a previous report of 2350 m s$^{-1}$ at 21°C[10]. For a

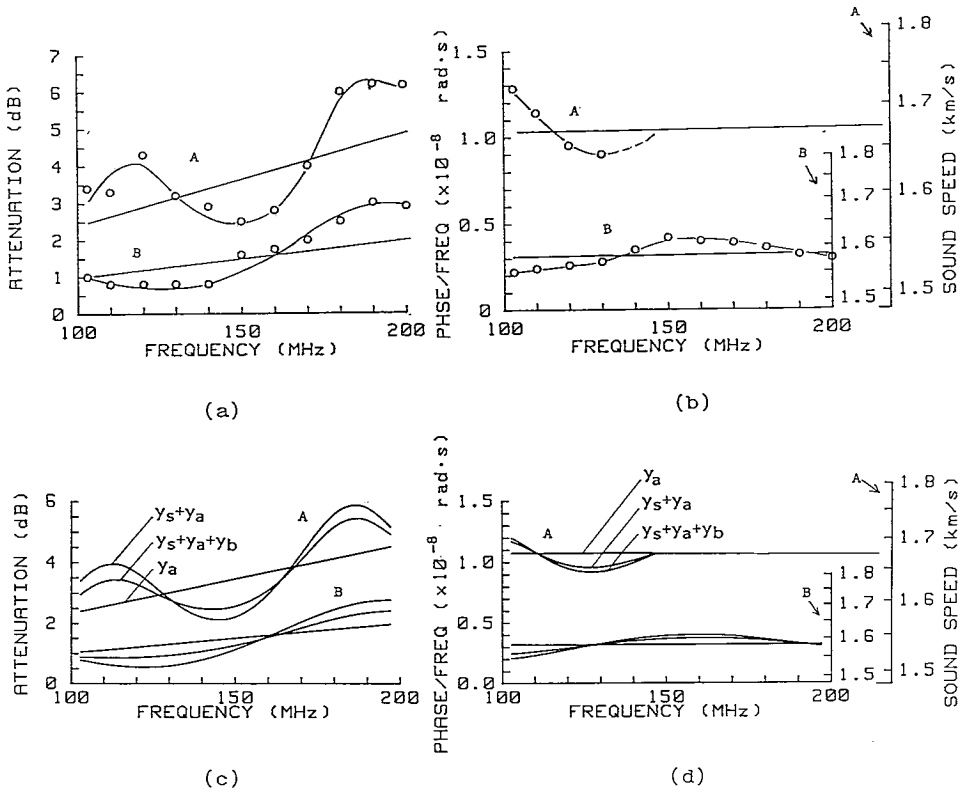


**Figure 7** Experimental data (a) and (b) and calculations (c) and (d) of the attenuation and the phase shift divided by frequency for tissues. Curve A, a part of scar areas in a human stomach (cancer); curve B, a part of hepatic lobular areas of a rat liver. In calculation A: $l_0 = 11$ $\mu$m, $\alpha = 100$ dB/mm at 100 MHz, $C_s = 1670$ m/s. B: $l_0 = 6$ $\mu$m, $\alpha = 80$ dB/mm at 100 MHz, $C_s = 1580$ m/s. The values substituted here were determined to fit the measurement data, and therefore, these are also results of the measurement. In calculation, the angle range 0° to 19° ($j$:0 to 40) was substituted for curve B, and the range 0° to 15° ($j$:0 to 32) was used for curve A

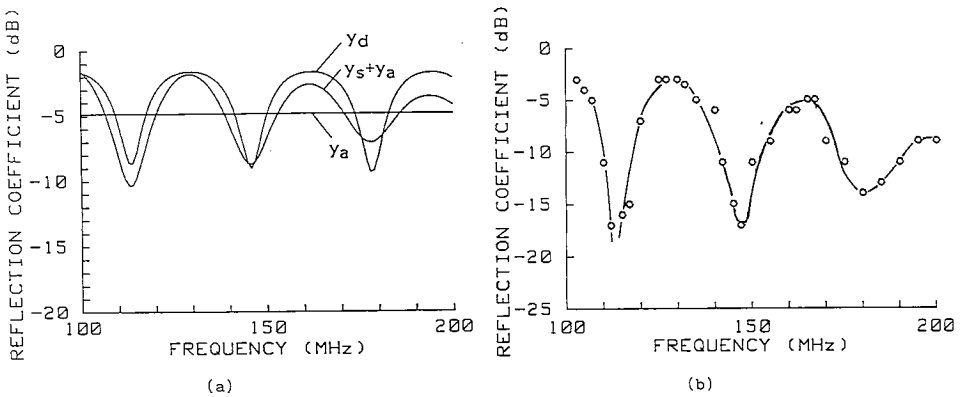


**Figure 8** Reflection coefficient of 37 $\mu$m thick polyester film mounted on a glass substrate. (a) Calculation of reflection coefficients as suggested in *Figure 6*. $\alpha$: attenuation coefficient, $2 \times 10^{-14} f^2$ neper m$^{-1}$ ($f$ in Hz); $C_s$: sound speed, 2400 m s$^{-1}$; $y_s + y_a$ and $y_d$ in this figure are normal incident waves; $y_d$ includes multiple reflection, determined from complete wave treatment for normal incidence. (b) Experimental data at 24°C

sound speed of 2400 m s$^{-1}$, large angle incident waves refract out of the receiving region. For this reason, the calculation in *Figure 8* was carried out only for normal incidence. The trace $y_d$ is the reflection coefficient calculated from the complete wave treatment (including multiple reflections), and the trace $y_s + y_a$ is given by

$$y_s + y_a = m_1 R_{12} + y_a \,|\, \theta_j = 0 \tag{18}$$

where $m_1$, the correction factor for the decrease of the acoustic pressure due to off-focus positioning, was determined as follows.

A focused wave is used so that the magnitude of the wave reflected from the plane surface located at an axial off-focus position, that is, the front surface of medium II, is less than that at the focal position; the boundary between media II and III. This variation along the beam axis is estimated by the relative reflected power profile shown in *Figure 3*. For example, the factor $m$ at 37 $\mu$m from the focal point is determined by regression analysis of the four points of interest at 37 $\mu$m; the intersection of $z = 37$ on the 160, 140, 120 and 103 MHz curves, to be

$$m = 0.457 \exp(0.017F) \text{ dB} \tag{19}$$

(where $F$ is the frequency in MHz) and

$$m_1 = 10^{-m/20} \tag{20}$$

The calculation in *Figure 8* shows that undulation maxima and minima appear at the same positions for $y_d$ and for $y_s + y_a$, and that the magnitude of undulation for $y_d$ remains constant, while the measured values show that magnitude of the undulation decreases with increasing frequency, suggesting that the reflected wave has components similar to those of $y_s + y_a$. The reason that the absolute values of the measurement are less than those of the calculation are associated with the transmission loss at the adhesive layer and the refraction loss of waves of large incident angles.

As a result, in the calculation for the measurement described later for this instrument, it will be considered that the components of the reflected waves are the wave $y_a$, reflected from the back surface, and the wave $y_b$ reflected from the front surface of the specimen.

Water was used as the coupling liquid. The attenuation of ultrasound traveling 20 $\mu$m distance in water at 20°C is approximately 0.18 dB at 200 MHz, calculated using the relation $\alpha/f^2 = 25.3 \times 10^{-17}$ s$^2$ cm$^{-1}$ (ref. 11), while that in the tissue used here is more than 2 dB, so that the contribution to the attenuation by water in the path can be neglected.

In the analysis below, the following equations are used for the reflected wave $y$

$$y = y_s + y_a \tag{21}$$

where

$$y_a = T_{12} R_{23} T_{21} \exp(-2\gamma_2 l_0) \tag{22}$$

$$y_s = m_1 R_{12} \tag{23}$$

$$y_{ref} = R_{13} \exp(-j2\beta_1 l_0), \tag{24}$$

the factor $m_1$ is given by equations (19) and (20), and the factor $m$ at 10 $\mu$m is 0.004 exp(0.029$F$).

## Attenuation and phase shift of the reflected wave

The back surface of the specimen is considered to be flat due to its intimate contact with the glass substrate, but the front surface, which is free from constraint, may not be flat microscopically because individual tissue elements of the specimen possess varying mechanical properties and may appear as suggested in *Figure 9*. However, there

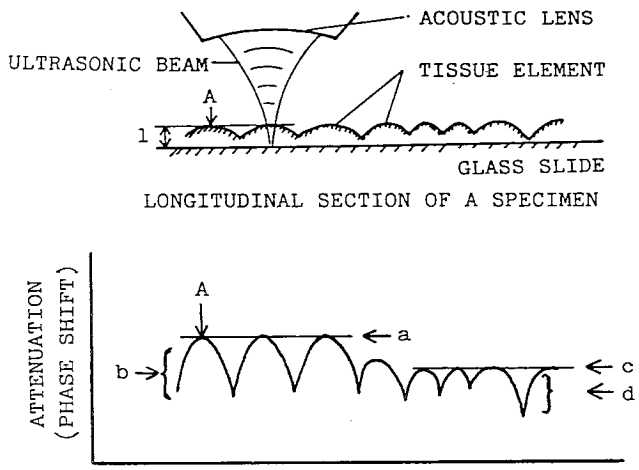


**Figure 9** Hypothetical model to discuss the relationship between longitudinal section of a specimen and the beamwidth. The front surface of the portion at maximum attenuation or phase shift of an A-mode in a tissue element is parallel to the glass substrate. Thickness of this portion is adopted for the specimen thickness

are limited regions for which the front surface may be considered to be parallel to the substrate surface, such as the section labeled A in *Figure 9* at which attenuation, or phase shift, becomes maximum at that point. The regions labelled b and d correspond to non-parallel thinner portions. That is, the levels a and c in *Figure 9* can be chosen to determine attenuation, or phase shift, and specimen thickness.

By using equations (21)–(24), attenuation and phase shift of the reflected wave are calculated to obtain characteristic patterns of frequency dependence as shown in *Figure 10*. The numerical values employed are listed in *Table 2*. In the calculation, it was assumed, for the tissue model, that the frequency exponent in the attenuation coefficient was unity and that the sound speed was non-dispersive. In *Figure 10*, the undulating curves are the attenuation or phase shift for $y_s + y_a$, and the straight lines, averaging the values of undulation, are those for the round trip wave $y_a$. Additionally, the attenuation and phase of the wave $y_a$ varies linearly with frequency. However, the reflected waves undulated due to the

**Table 2** Values substituted to calculate attenuation and phase shift of a tissue model

| | |
|---|---|
| Attenuation coefficient | $\alpha_2 = 1.151 \times 10^{-4} f$ (neper $m^{-1}$) ($f$ in Hz) (from 100 dB $mm^{-1}$ at 100 MHz, assumed slope of unity) |
| Sound speed | $C_s = 1550$–$1750$ m $s^{-1}$ (assumed non-dispersive) |
| Specimen thickness | $l = 8$–$12$ $\mu$m |

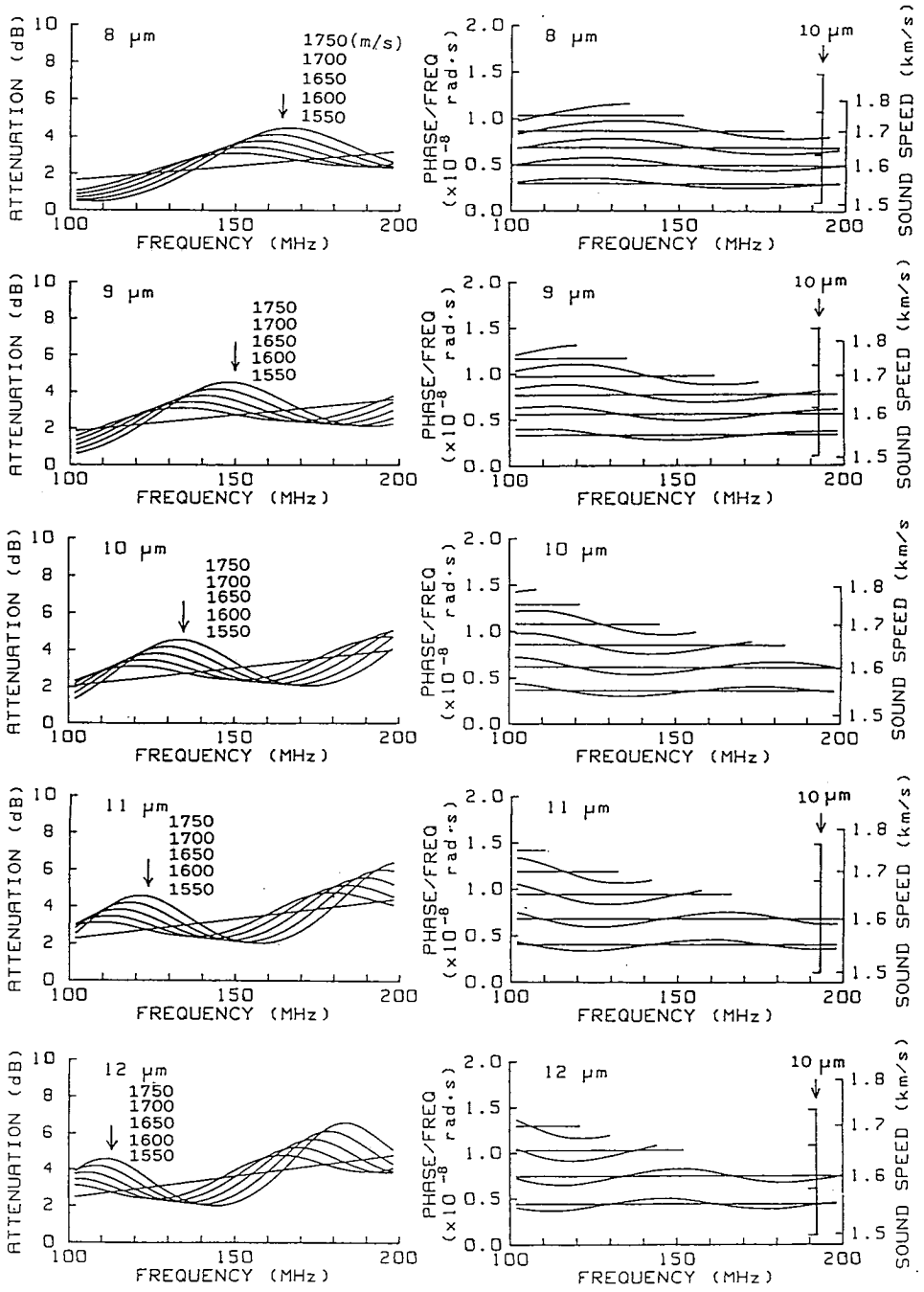


**Figure 10** Calculation of attenuation and phase shift of the reflected wave from the model of *Figure 5*. Thickness $l_0 = 8$–$12$ $\mu$m. The composite wave of $y_s + y_a$ undulates the traces, although the wave $y_a$ itself varies linearly with frequency. These straight lines strictly reveal attenuation and sound speed

addition of the wave $y_s$. This undulation depends significantly upon specimen thickness.

## Simultaneous measurement of thickness, attenuation constant and sound speed

The ideas of the previous section can be used to determine the actual thickness of biological tissues by the non-contact procedure, if the experimental data obtained are similar to the theoretically determined patterns shown in *Figure 10*. The actual thickness is determined by comparing positions of the maxima or minima of the graphs of attenuation or phase shift. For example, if the attenuation curve has a maximum in the frequency range 120 to 135 MHz, a minimum in the range 150 to 170 MHz, and the phase curve has maxima in the neighbourhood of 100 MHz and minima in the range 135 to 145 MHz, it can be judged that the thickness is 10 $\mu$m. The actual attenuation and phase shift in the tissue are determined by the straight line corresponding to attenuation or phase shift of the wave $y_a$ in the path length $2l_0$. Thus, with the thickness determined, the attenuation constant can be obtained by normalizing the attenuation value by twice the thickness and the sound speed $C_s$ can be read directly from the speed scale in the right side of the phase graph.

## Measurement

The sample tissue were formalin fixed, paraffin embedded and sectioned with a microtome to a thickness of 10 $\mu$m for the acoustic microscope and 3 $\mu$m for the light microscope. The sectioned specimen was mounted on a glass substrate and then the paraffin was removed. Water (20°C) was used for the coupling medium between the lens and the specimen. The sample for the light microscope was stained with Elastica Masson to aid in determining types of tissue elements.

In the experimental data shown in *Figure 11*, attenuation $L$ was obtained from

$$L = -(10 \log(y_s + y_a)^2 - 10 \log y_{ref}^2) \quad (25)$$

instead of equation (13) and the phase shift was obtained from equation (16). In this way, the difference between the reflection coefficients at the boundaries between water and the substrate, and between the tissue specimen and the substrate, is approximately 0.2 dB and this becomes the principal error, particularly at low frequencies where the total attenuation is less. For instance, if attenuation in the specimen at 100 MHz is 1.5 dB, the error of 0.2 dB is approximately 13%.

The points plotted in *Figure 11* are the measurements for three samples of infarcted myocardium. It is seen that there is a significant variation in the data as a function of frequency, and from sample to sample. For instance, regarding the collagenous fibre tissues Fc (marked ○ in the figure), the values of attenuation at 130 MHz for samples a, b and c are 2.5, 5 and 3 dB, respectively. Thus the total range of values is larger than 200%. Moreover,

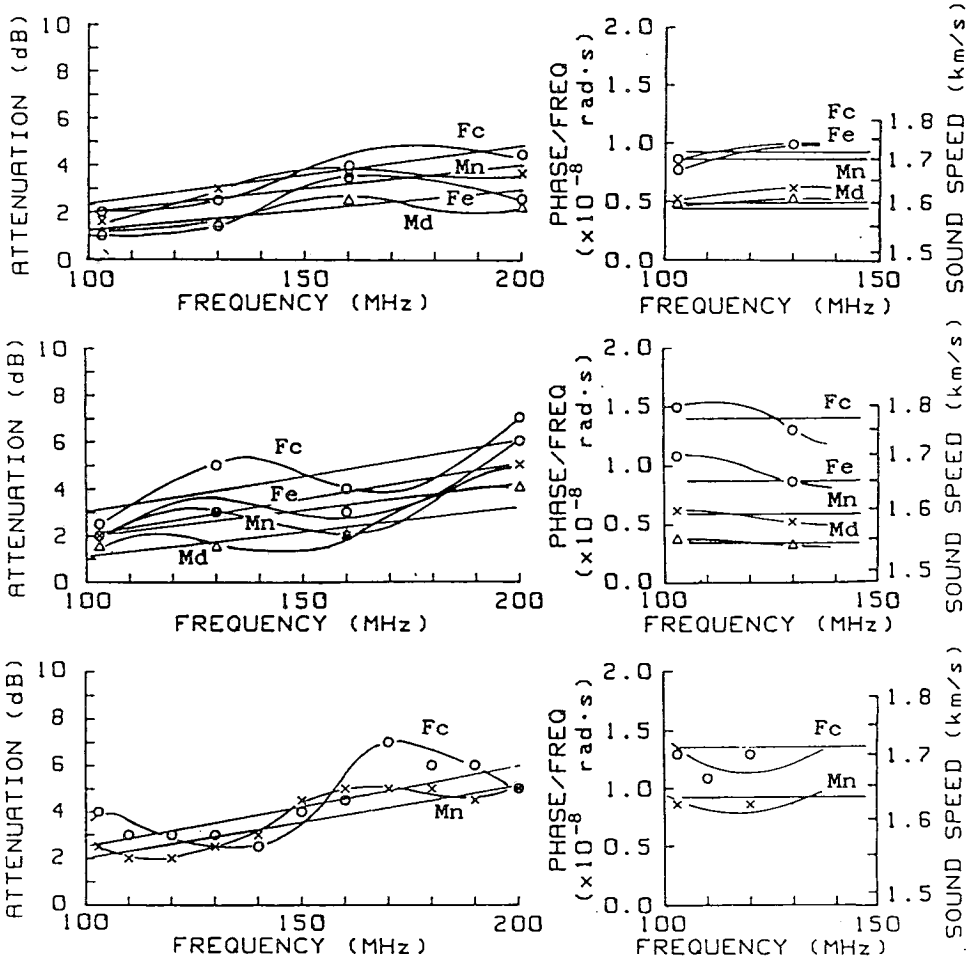


**Figure 11** Experimental data of attenuation and phase shift in the tissue sections of three infarcted myocardia (a, b, c). Mn: normal cardiac muscles area (×); Md: degenerated cardiac muscles area (△); Fc: collagenous changed area (○); Fe: elastic changed area (○). (after reference 5)

**Table 3** Experimental data, attenuation constant and sound speed of the tissue sections, around 10 $\mu$m thick, cut from three infarcted myocardia of human origin, one paraffin embedded, in the frequency range 100 to 200 MHz (20°C)

| | | Attenuation (dB mm$^{-1}$) | | Slope | Sound speed (m s$^{-1}$) |
|---|---|---|---|---|---|
| | | 100 MHz | 200 MHz | | |
| Example 1 *Figure 11a* | | | | | |
| Mn | × | 125 | 250 | 1 | 1600 |
| Md | △ | 80 | 190 | 1.2 | 1580 |
| Fc | ○ | 150 | 300 | 1 | 1710 |
| Fe | ○ | 80 | 190 | 1.2 | 1700 |
| Example 2 *Figure 11b* | | | | | |
| Mn | × | 100 | 200 | 1 | 1590 |
| Md | △ | 70 | 150 | 1.1 | 1540 |
| Fc | ○ | 150 | 300 | 1 | 1770 |
| Fe | ○ | 100 | 250 | 1.3 | 1650 |
| Example 3 *Figure 11c* | | | | | |
| Mn | × | 80 | 200 | 1.3 | 1630 |
| Fc | ○ | 100 | 240 | 1.3 | 1710 |

for sample a, the attenuation of Fc is less than that of the area of normal cardiac muscle Mn, however, for samples b and c, the attenuation of Fc is greater than that of Mn.

Although the microtome was set to section the tissues at a thickness of 10 $\mu$m, it is considered that the variations in the data in *Figure 11* are due to the variations of specimen thickness. Thus, the data of *Figure 11* can be explained as follows.

For example, for the sample shown in *Figure 11a*, the attenuation curves have minima below 120 MHz and maxima in the range 150–170 MHz and the phase shift at 130 MHz is greater than that at 100 MHz. These facts, compared with the theoretical calculations in *Figure 10*, showed the thickness of the specimen to be 8 $\mu$m. As for samples shown in *Figure 11(b)* and (*c*), the thicknesses were determined to be 10 and 12 $\mu$m, respectively, by the same procedure, comparison of positions of maxima and minima. The attenuation and sound speed thus obtained were depicted by the straight lines in the same figure. The results are listed in *Table 3*.

The experimental data from 49 regions of the above three infarcted and one normal myocardium samples were analysed by this method and the results were summarized in *Table 4*.

Thus, once the data were obtained experimentally, the specimen thickness was determined and the attenuation constant and sound speed were obtained. Consequently, as shown in *Tables 3* and *4* tissue elements were studied and characteristic acoustic properties were obtained, which demonstrates the utility of the method.

## Discussion

Although the microtome was set to section tissues at 10 $\mu$m, the actual thicknesses varied between 8 to 12 $\mu$m. Because thickness measurements of more than three areas which are distant from each other by more than 1 cm were shown to be the same value in 0.5 $\mu$m steps, it is considered that the thickness variation in one section was less than this range.

With respect to attenuation, it was assumed for the tissue model that the frequency exponent in the attenuation coefficient was unity. This was somewhat justified by the measurements in that nearly all of the exponents of the frequency dependence of attenuation varied from 1.0 to 1.3 as shown in *Table 3*. The fraction of the components of large incident angle increase with frequency. This may be one of the reasons why the exponent becomes greater than unity.

The attenuation obtained by equation (25), in practice,

**Table 4** Experimental data of attenuation constant and sound speed of myocardia (20°C). The data were obtained from 49 regions in the tissue sections of three infarcted (*Table 3*) and one normal myocardia

| | Attenuation (dB mm$^{-1}$) | | Speed (m s$^{-1}$) |
|---|---|---|---|
| | 100 MHz | 200 MHz | |
| Cardiac muscle | | | |
| normal area | | | |
| longitudinal | 80–120 | 200–300 | 1600–1650 |
| transverse | 60–100 | 160–200 | 1590–1630 |
| degenerated area | 30– 80 | 80–200 | 1520–1600 |
| collagenous changed area | 100–160 | 250–320 | 1660–1770 |
| elastic changed area | 90–100 | 200–260 | 1650–1700 |
| mixed area of collagenous and elastic fibres | 100–160 | 250–300 | 1660–1800 |

includes the mismatch loss at the boundary between the coupling medium and the tissue, the loss arising in propagation in the tissue and the reflection loss at the glass substrate. The contribution of the first loss to the transmitted wave $y_a$ is less than 1%, and considered negligible. Though the attenuation value by the reflection loss is compensated by the reference wave, the method in practice in equation (25) produces a principal error of approximately 10%, particularly at the lower frequencies. Consequently, the attenuation values listed in *Tables 3* and *4* show the propagation loss basically due to absorption and scattering with the error approximately 10%.

As to dispersion of sound speed in biological tissues, some observations have been reported[12–14]. Kremkau *et al.*[14] observed speed dispersion in human brain to be approximately 1 m $s^{-1}$ $MHz^{-1}$ in the frequency range 1–5 MHz. However, the experimental graph in their study also shows the speed increasing linearly with the logarithm of frequency. If such a dependence also occurs in the range 100–200 MHz, the sound speed would increase approximately 2 m $s^{-1}$. That is, in this frequency range, sound speed dispersion would not be observable because the measurement method is a procedure for estimating from the frequency characteristics of attenuation and phase shift and not accurate to 2 m $s^{-1}$. The sound speed was not observably dispersive in the frequency range 100–200 MHz. The assumption that sound speed was non-dispersive was thus somewhat justified.

The advantage of the measurement procedure is that once the amplitude and phase data are taken, the values of thickness, attenuation constant and sound speed can be obtained for tissue elements without additional measurements. This resolves the problem caused because the thickness of a thin biological tissue cannot be determined by a contact method.

In obtaining the data as described here, considerable time is required for processing a single sample, including reading the levels of amplitude and phase as shown in *Figure 4*, drawing the graphs of frequency characteristics as shown in *Figures 7* and *11*, curve fitting, and determining specimen thickness, attenuation and sound speed. However, automated processing is possible, and, in fact, is being developed such that single sample processing can be completed within several hours.

In the present study, formalin fixed, paraffin embedded tissue was used. It has been found that formalin fixation increases both attenuation and sound speed, to some extent[15]. This may be related to alteration of the structure in the tissue at the macromolecular level. The acoustic properties of paraffin embedded tissue could not be measured as the attenuation of paraffin is much greater than that of tissue. The attenuation and sound speed of a tissue after removing paraffin could be measured even though the attenuation is greater than that of fixed tissue. Complete data for the change in acoustic properties introduced by fixation, embedding and removal of embedding material have not been obtained in detail.

In scanning the transducer mechanically over the 2 mm excursions, the transducer does not move in a perfectly straight path and the surface of the glass substrate is not perfectly flat. For this reason, some error occurs in phase data. In order to reduce this error, the glass of a high degree of flatness was found to be superior to that generally used in light micoscopy. A later modification of the present study involves deleting undesirable phase shift data associated with imperfectly straight scans using computer processing.

## Acknowledgements

This study was supported, in part, by the Ministry of Education, Science and Culture of Japan, by the Japan–United States Cooperative Science Program of JSPS (Japan), NSF (USA) and by NIH (USA). The authors are grateful to N. Chubachi, J. Kushibiki and T. Sannomiya, Faculty of Engineering, Tohoku University and to W.D. O'Brien Jr, Bioacoustics Research Laboratory, the University of Illinois for discussions on acoustics and to T. Takahashi, N. Tamahashi (Section of Pathology), M. Suzuki, I. Abe (Section of Oncology) at Research Institute for Chest Diseases and Cancer, Tohoku University for discussion on pathology and histology. The authors also acknowledge the Honda Electronics Company (Japan) for assistance in the trial production of the SAM instrument.

## References

1 **Kessler, L.W., Palermo, P.R. and Korpel, A.** Practical high resolution acoustic microscopy *Acoustical Holography* (Ed. Wade, G.) (1972) **4** 51–71

2 **Tervola, K.M.U., Foster, S.G. and O'Brien, W.D. Jr.** Attenuation coefficient measurement technique at 100 MHz with the scanning laser acoustic microscope *IEEE Trans Sonics Ultrason* (1985) **SU-32** 259–265

3 **Lee, C.C., Tsai, C.S. and Cheng, X.** Complete characterization of thin- and thick-film materials using wideband reflection acoustic microscopy *IEEE Trans Sonics Ultrason* (1985) **SU-32** 248–258

4 **Tanaka, M., Okawai, H., Chubachi, N. and Kushibiki, J.** Studies on the non-contact method for the measurement of acoustic properties of tissue *Proc 48th Mtg Jpn Soc Ultrason Med* (1986) 667–668 (In Japanese)

5 **Okawai, H., Tanaka, M., Chubachi, N. and Kushibiki, J.** Non-contact simultaneous measurement of thickness and acoustic properties of a biological tissue using focused wave in a scanning acoustic microscope *Proc 7th Symp Ultrason Elect Kyoto Jpn J Appl Phys* (1987) **Suppl 26-1** 52–54

6 **Lemons, R.A. and Quate, C.F.** A scanning acoustic microscope *Ultrason Symp Proc IEEE cat73* (1973) **CHO-807-BSU**, 18–21

7 **Tanaka, M., Okawai, H., Chubachi, N., Kushibiki, J. and Sannomiya, T.** Development of an acoustic microscope for medicine *Proc 45th Jpn Soc Ultrason Med* (1984) 677–678 (In Japanese)

8 **Tanaka, M., Okawai, H., Chubachi, N., Kushibiki, J., Takahashi, T. and Hashimoto, K.** Development of acoustic microscope for the medical and biological use and its medical application *Kokenshi* (*Kosankinbyo kenkyusho Zasshi*) (1985) **37** 377–387 (in Japanese)

9 **Chubachi, N., Kushibiki, J. and Sannomiya, T.** Scanning acoustic microscope employing concave ultrasonic transducers *Proc 1st Symp Ultrason Elect Tokyo, Jpn J Appl Phys* (1981) **Suppl 20-3** 73–76

10 **Chubachi, N. and Sannomiya, T.** Reflection mode acoustic interference microscope. Reports of spring meeting, Acoustic Society of Japan 1984 (1984) 621–622 (in Japanese)

11 **Pinkerton, J.M.M.** The absorption of ultrasonic waves in liquids and its relation to molecular constitution *Proc Phys Soc* (1949) **B62**, 129–141

12 **Carstensen, E.L. and Schwan, H.P.** Acoustic properties of hemoglobin solutions *J Acoust Soc Am* (1959) **31** 305–311

13 **O'Donnell, M., Jaynes, E.T. nd Miller, J.G.** General relationships between ultrasonic attenuation and dispersion *J Acoust Soc Am* (1978) **63** 1935–1937

14 **Kremkau, F.W., Barnes, R.W. and McGraw, C.P.** Ultrasonic attenuation and propagation speed in normal human brain *J Acoust Soc Am* (1981) **70** 29–38

15 **Bamber, J.C., Hill, C.R., King, J.A. and Dunn, F.** Ultrasonic propagation through fixed and unfixed tissues *Ultrasound Med Biol* (1979) **5** 159–165

16 **Greenspan, M. and Tschiegg, C.E.** Tables of the speed of sound in water *J Acoust Soc Am* (1958) **31** 75–76